JOURNAL OF APPLIED CRYSTALLOGRAPHY
ISSN 1600-5767

Structural chirality and natural optical activity across the α to β phase transition in SiO_2 and $AlPO_4$ from first principles

Fernando Gómez-Ortiz,[a]* Asier Zabalo,[a] A. Mike Glazer,[b] Emma E. McCabe,[c] Aldo H. Romero[d] and Eric Bousquet[a]*

[a]Theoretical Materials Physics, Q-MAT, Université de Liège, B-4000 Sart-Tilman, Belgium, [b]Department of Physics, Oxford University, Parks Road, Oxford OX1 3PU, United Kingdom, [c]Department of Physics, Durham University, South Road, Durham DH1 3LE, United Kingdom, and [d]Department of Physics and Astronomy, West Virginia University, Morgantown, WV 26505-6315, USA. *Correspondence e-mail: fgomez@uliege.be, eric.bousquet@uliege.be

Received 3 October 2025
Accepted 9 January 2026

Edited by J. Harper, University of Utah, USA

Keywords: chirality; natural optical activity; quartz.

Natural optical activity (NOA), the ability of a material to rotate the plane of polarized light, has traditionally been associated with structural chirality. However, this relationship has often been oversimplified, leading to conceptual misunderstandings, particularly when attempts are made to correlate structural handedness directly with optical rotatory power. In reality, the relationship between chirality and NOA is more nuanced: optical activity can arise in both chiral and achiral crystal structures, and the sign of the rotation cannot necessarily be inferred from the handedness of the space group. In this work, we conduct a first-principles investigation of NOA in SiO_2 and $AlPO_4$ crystals, focusing on their enantiomorphic structural phase transition from high-symmetry hexagonal ($P6_422$ or $P6_222$) to low-symmetry trigonal ($P3_121$ or $P3_221$) space groups. This transition, driven by the condensation of a zone-centre Γ_3 phonon mode, reverses the screw-axis type given by the space-group symbol while leaving the sign of the optical activity unchanged. By following the evolution of the structure and the optical response along the transition pathway, we clarify the microscopic origin of this behaviour. We demonstrate that the sense of optical rotation is determined not by the nominal handedness of the screw axis given in the space-group symbol but by the atomic-scale handedness of the most polarizable atoms of the structure.

1. Introduction

Natural optical activity (NOA) was first observed in the early 19th century by Arago (1811) and Biot (1812) when they discovered that certain materials could rotate the plane of polarization of light. Because atomic theory and electromagnetic theory were still nascent, the microscopic cause of this rotation and its broader significance remained unclear at the time. Since then, there have been several attempts to give a microscopic explanation of how NOA emerges in certain materials. Many theories have been developed (Condon, 1937; Natori, 1975; Zhong *et al.*, 1993; Barron, 2009; Pozo Ocaña & Souza, 2023), either applying electromagnetic theory or relying on atomic polarizabilities, as described by Kizel' (1980). Currently, NOA is understood as a formal representation of the initial spatial dispersion of the macroscopic permittivity tensor as described by first-order principles (Landau & Lifshitz, 1984; Agranovich & Ginzburg, 1984). Moreover, it has recently become efficiently and conveniently computationally accessible through first-principles density functional perturbation theory in both molecular and solid states (Zabalo & Stengel, 2023). Finally, from an experimental point of view, NOA manifests itself through optical rotation,

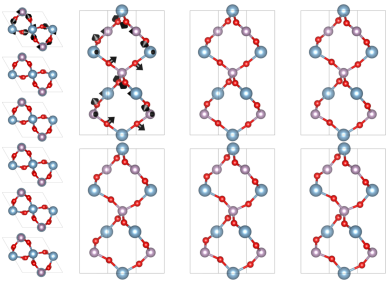

which can be measured by the rotation angle of the orientation of the plane of polarization about the optical axis of linearly polarized light as it travels through certain materials (Jerphagnon & Chemla, 1976; Condon, 1937; Bousquet *et al.*, 2025; Nomura, 1960; Ades & Champness, 1975; Iwasaki *et al.*, 1972).

While it is a well known fact that NOA is frequently linked with structural chirality, it is currently understood that chirality is a sufficient, but not necessary, condition for NOA to occur, given that achiral materials can also display NOA characteristics (Halasyamani & Poeppelmeier, 1998; Fecher *et al.*, 2022; Bousquet *et al.*, 2025). This historical association led to the widespread belief that the handedness of a material's space group directly determines the handedness of its optical rotation (Wooster, 1953; Gómez-Ortiz *et al.*, 2024). Although this correlation may hold in many cases, the reality is more nuanced: the direction of optical rotation does not necessarily follow the handedness given in the space-group symbol (Glazer & Stadnicka, 1986; Glazer, 2018).

Measurements of optical activity are a common practice for organic chiral molecules (*e.g.* sugars or tartaric acid) and, although comparatively weaker, it remains measurable in inorganic crystals such as low quartz and berlinite (Glazer & Stadnicka, 1986). Quartz (SiO_2) adopts a trigonal structure [enantiomorphic space groups $P3_121$ (No. 152) or $P3_221$ (No. 154)] at room temperature (α-quartz) and transforms sharply to hexagonal β-quartz [enantiomorphic space groups $P6_422$ (No. 181) or $P6_222$ (No. 180), respectively] at 573°C; both polymorphs are chiral despite being built from achiral SiO_4 tetrahedra. Berlinite ($AlPO_4$), a structural analogue of quartz, similarly undergoes an $\alpha \rightarrow \beta$ transition at approximately 586°C, passing from trigonal $P3_121$ ($P3_221$) symmetry to hexagonal $P6_422$ ($P6_222$) without disrupting the network of corner-sharing tetrahedra (Ng & Calvo, 1976; Shapiro *et al.*, 1967; Grimm & Dorner, 1975). In such transitions, the sense of the principal screw axis of the space-group symbol reverses sign, but the sense of the optical activity of the crystal remains unchanged (Donnay & Le Page, 1978; Glazer, 2018). Initially, this might appear counterintuitive but, as discussed by Glazer & Stadnicka (1986), the direction of rotation for the chain composed of the most polarizable atoms actually determines the direction of optical activity. In quartz we find two small-channel right-handed helices and one non-symmetric large-channel left-handed helix that are preserved throughout the transition. This arrangement of helices endows quartz with a chiral bivector (Hlinka, 2014; Erb & Hlinka, 2018). Right- and left-handed helices have the same number of atoms per unit volume. Since there are two right-handed helices to one left-handed helix that are preserved throughout the transition (although they may be slightly distorted, losing perfect symmetry and no longer conforming to a sixfold helix), the optical activity is preserved despite the reversal of the principal screw axis in these crystal structures.

In this work, we aim to carry out an in-depth first-principles investigation of this structural transition and, following the workflow presented by Gómez-Ortiz *et al.* (2025), we show that it can be associated with the progressive condensation of a zone-centre Γ_3 phonon mode consistent with symmetry analysis of rotations of SiO_4 units (Campbell *et al.*, 2018). By following the evolution of the crystal structure from the high-symmetry (HS) to the low-symmetry (LS) enantiomorphic phase, we track how both the screw axis and the NOA evolve along the transition path, providing microscopic insight into the interplay between chirality, lattice dynamics and optical rotation.

2. Computational details

For all the calculations, we converged the structural data of the parent structure with the *Abinit* code (Version 9.10.5; Gonze *et al.*, 2020) with the PBEsol exchange-correlation functional. We used the plane wave pseudopotential approach with optimized norm-conserving pseudopotentials as taken from the *PseudoDojo* server (Version 4; Hamann, 2013; Van Setten *et al.*, 2018) and an energy cutoff of 40 hartrees. The k-mesh sampling employed for the calculations was $6 \times 6 \times 6$ for both the structural relaxations and the computation of the NOA. A value of 10^{-6} hartrees per bohr was employed on the forces to stop the structural relaxations, and a value of 10^{-7} hartrees was used for the electronic residual self-consistent cycle stop. Phonon calculations were computed through the density functional perturbation theory framework as implemented in *Abinit* (Gonze & Lee, 1997; Gonze *et al.*, 2020).

For the calculation of the optical activity, we focus on the low-frequency limit of $\overline{\rho}(\omega) = \rho(\omega)/(\hbar\omega)^2$, which tends to a constant as $\omega \rightarrow 0$, where $\rho(\omega)$ is the rotatory power and $\hbar$ the reduced Planck constant. For both SiO_2 and $AlPO_4$, we assume that the incident light propagates along the optical axis, which is considered to be parallel to the z Cartesian direction. Under these conditions, $\overline{\rho}(0) \simeq \eta_{xyz}/[2(\hbar c)^2]$, where c is the speed of light and η_{xyz} is a component of the NOA tensor in the zero frequency limit. While numerous methodologies and strategies for computing the NOA in solids exist (Natori, 1975; Zhong *et al.*, 1993; Malashevich & Souza, 2010; Pozo Ocaña & Souza, 2023; Wang & Yan, 2023; Urru *et al.*, 2025), this study utilizes the latest linear response approach grounded in density functional perturbation theory developed by Zabalo & Stengel (2023) and incorporated into *Abinit*.

3. Results

3.1. Structural transition of SiO_2 and $AlPO_4$

Let us start by analysing the high-symmetry phase of SiO_2, which crystallizes in the enantiomorphic $P6_422$ (or $P6_222$) space group. For simplicity, we restrict our analysis to the $P6_422$ structure, as the methodology for the other space group is analogous and yields identical conclusions.

This structure is characterized by a network of corner-linked SiO_4 tetrahedra arranged about a principal screw axis aligned with the crystallographic c axis, as shown in Fig. 1. Notably, the crystallization process fixes the chirality into the $P6_422$ (or $P6_222$) space group and the associated properties.

Table 1
Relaxed DFT structural data (atom position along x, y and z directions) in reduced coordinates for the high-symmetry phase ($P6_422$) of SiO_2.

The calculated cell parameters of the $P6_422$ structure are $a = b = 5.074$ Å and $c = 5.554$ Å.

Atom	x	y	z
Si (3*d*)	0.0000	0.5000	0.3333
O (6*i*)	0.2080	0.4160	0.5

Table 2
Relaxed DFT structural data (atom position along x, y and z directions) in reduced coordinates for the low-symmetry phase ($P3_121$) of SiO_2.

The calculated cell parameters of the $P3_121$ structure are $a = b = 4.951$ Å and $c = 5.441$ Å.

Atom	x	y	z
Si (3*a*)	0.0000	0.4689	0.6666
O (6*c*)	0.1442	0.7308	0.4515

Recently, an algorithm has been proposed to identify chiral displacive transitions from achiral to chiral space groups (Gómez-Ortiz *et al.*, 2025), following the work of Fava *et al.* (2024) for K_3NiO_2. Applying this workflow (Gómez-Ortiz *et al.*, 2025) to SiO_2 and $AlPO_4$, we find that a displacive phase transition from an achiral to a chiral space group is not allowed by pseudosymmetry. In other words, no achiral phase lies sufficiently close to the chiral phases of SiO_2 or $AlPO_4$ to permit a displacive transition.

However, symmetry considerations predict that the high-symmetry $P6_422$ right-handed screw-axis structure can be linked to the low-symmetry $P3_121$ left-handed screw-axis structure (Shapiro *et al.*, 1967; Grimm & Dorner, 1975) through the Γ_3 irrep of the zone centre (Antao, 2016; Campbell *et al.*, 2018) (or similarly between the $P6_222$ and the $P3_221$ space groups). This distortion removes 6_4 symmetry, leaving a 3_1 screw, as shown by the shaded hexagon and double triangles in Fig. 1. This means that those two space groups can form a high-symmetry/low-symmetry pair for SiO_2 or $AlPO_4$.

From our density functional theory (DFT) calculations, we confirm the presence of an unstable phonon mode at the Γ point in the $P6_422$ phase of SiO_2, as referenced by Raman & Nedungadi (1940). By checking the corresponding phonon eigenvector symmetry, we found that it has the Γ_3 irrep, *i.e.* in agreement with the symmetry analysis which links the right-handed screw of the high-symmetry phase and the left-handed screw of the low-symmetry phase. Such a mode is neither Raman nor infrared active, *i.e.* it is silent, as reported some time ago through hyper-Raman (Tezuka *et al.*, 1991) or inelastic neutron scattering (Axe & Shirane, 1970). Hence, these results go in the direction of the displacive character of the transition (Choudhury & Chaplot, 2006), helping clarify previous discussions of its nature (Dolino *et al.*, 1983). The calculated structural data of the converged $P6_422$ structure computed with a k-mesh of $6 \times 6 \times 6$ can be found in Table 1. From our density functional perturbation theory calculations, we found that the unstable imaginary frequency of the Γ_3 mode has an amplitude of $61i$ cm^{-1}. The condensation and relaxation of the Γ_3 eigenvector give an energy difference between the high- and low-temperature phases of $\Delta E = -60$ meV per nine atoms within the unit cell.

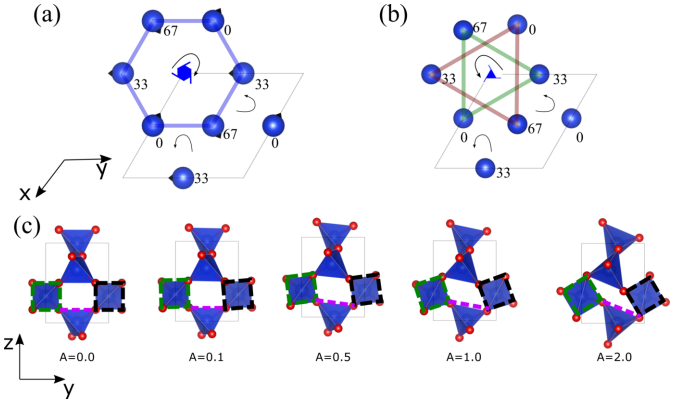

Figure 1
Top views of the in-plane structural distortion in SiO_2 from (*a*) the $P6_422$ space group to (*b*) the $P3_121$ space group, with the movements of the Si atoms represented by black arrows on the atoms. Curved arrows are a guide to the eye indicating the clockwise and counter-clockwise helices displayed by the Si atoms. (*c*) Side views illustrating the twisting of SiO_4 tetrahedra as a function of the Γ_3 mode amplitude. The amplitude $A = 1.0$ corresponds to the optimal distortion, yielding the maximum energy gain. The shaded hexagon in panel (*a*) and the double triangles in panel (*b*) illustrate how the 6_4 screw-axis symmetry is broken during the distortion.

A symmetry-adapted mode analysis of our relaxed low-symmetry phase using the *ISODISTORT* software (Stokes *et al.*, 2025; Campbell *et al.*, 2006) reveals that the distortion decomposes into Γ_1 and Γ_3 irreps, where the amplitude of the Γ_1 mode is marginal (0.03 Å) with respect to the leading Γ_3 mode (1.00 Å) which drives the transition. The Γ_3 mode induces in-plane displacements of the Si atoms and both out-of-plane and in-plane displacements of the O atoms. The displacements are such that the SiO_4 tetrahedra rotate as fairly rigid units (and do not distort significantly), as illustrated in Fig. 1(*c*). As shown in Figs. 1(*a*) and 1(*b*), the in-plane projection of the displacements induces a coordinated counter-clockwise and clockwise movement between the neighbouring helical centres. This movement breaks the 6_4-fold screw axis at the corners of the unit cells which transform into 3_1 centres while preserving the 3_1-fold screw axis at the interior of the unit cell. The structural data of the low-symmetry $P3_121$ structure are provided in Table 2.

Moving now to the case of $AlPO_4$, when studying its $P6_422$ phase, we can observe a similar crystal structure to that of the $P6_222$ phase of SiO_2 (Schwarzenbach, 1966; Muraoka & Kihara, 1997), with the exception that the c axis is essentially doubled due to the ordering of Al + P over the atom sites (as discussed below). The crystal structure is shown in Fig. 2. The calculated structural data of the converged $AlPO_4$ $P6_422$ structure can be found in Table 3. Similarly to the previous SiO_2 case, we also obtain an unstable phonon mode at the Γ point of the right-handed high-symmetry phase with an amplitude of $63i$ cm^{-1} and the irrep Γ_3 (Muraoka & Kihara, 1997). This Γ_3 mode thus gives the link between the right-

Table 3
Relaxed DFT structural data (atom position along x, y and z directions) in reduced coordinates for the high-symmetry phase ($P6_422$) of $AlPO_4$.

The relaxed cell parameters of the $P6_422$ phase are $a = b = 5.136$ Å, $c = 11.301$ Å.

Atom	x	y	z
Al (3*c*)	0.5000	0.0000	0.0000
P (3*d*)	0.5000	0.0000	0.5000
O (12*k*)	0.1938	0.4201	0.7560

Table 4
Relaxed DFT structural data (atom position along x, y and z directions) in reduced coordinates for the low-symmetry phase ($P3_121$) of $AlPO_4$.

The relaxed cell parameters of the $P3_121$ phase are $a = b = 4.983$ Å, $c = 11.024$ Å.

Atom	x	y	z
Al (3*a*)	0.4680	0.0000	0.3333
P (3*b*)	0.4682	0.0000	0.8333
O (6*c*)	0.1265	0.7104	0.2684
O (6*c*)	0.1598	0.7445	0.7821

handed high-symmetry and the left-handed low-symmetry chiral phases, again similarly to the case of SiO_2 but with a doubled cell along the z direction. The condensation and relaxation of the eigenvector of this Γ_3 unstable mode give, in this case, an energy gain of $\Delta E = -155$ meV per 18-atom unit cell, which is comparable to SiO_2 when normalized to the number of atoms. The relaxed structure we obtain is fully consistent with previous work (Thong & Schwarzenbach, 1979; Schwarzenbach, 1966). Similar conclusions to those drawn in the previous example can be reached by analysing the distortion induced by the Γ_3 mode, which causes in-plane displacements of the Al and P atoms and both in-plane and out-of-plane displacements of the O atoms as in the case of the quartz crystal. The symmetry-adapted mode decomposition gives amplitudes of 0.08 Å for the Γ_1 irrep and 1.57 Å for the Γ_3 irrep. The structural data of the low-symmetry $P3_121$ structure are provided in Table 4.

Hence, we have found with our calculations that both SiO_2 and $AlPO_4$ have an unstable phonon mode in their high-symmetry $P6_422$ (or $P6_222$) chiral phase that drives the phase transition towards the lower-temperature chiral structure $P3_121$ (or $P3_221$). We will now examine the connection between these phase transitions and their optical activity.

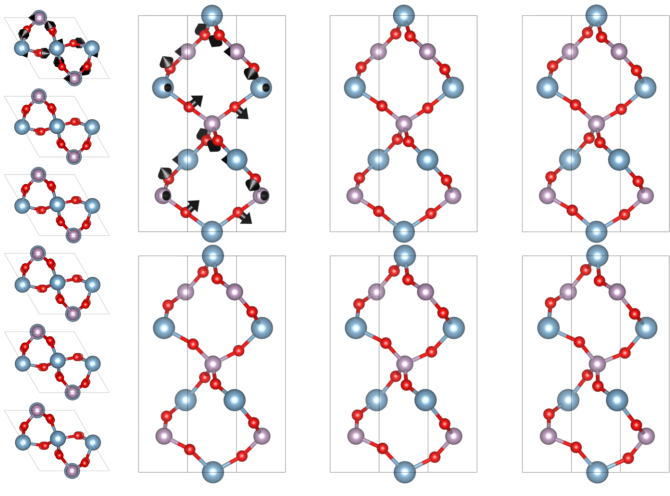

Figure 2
(First column) Top views and (second to fourth columns) side views of the progressive structural distortion in $AlPO_4$ from the $P6_422$ to the $P3_121$ space groups. The distortion amplitude increases from left to right and from top to bottom, in increments of 0.2, ranging from 0 (undistorted high-symmetry phase) to 1 (relaxed low-symmetry phase). Black arrows in the first panels indicate the directions of atomic displacements associated with the distortion. Red, blue and pink atoms correspond to O, Al and P, respectively.

3.2. Evolution of the NOA

To explore the microscopic origin of the optical activity in these systems, we now analyse the evolution of the NOA along the structural transition path from the high-symmetry to the low-symmetry enantiomorphic phases in both SiO_2 and $AlPO_4$.

The results are summarized in Fig. 3 and Table 5. The first interesting point emerging from our calculations is the opposite sign of the NOA in the high-symmetry high-temperature $P6_422$ phases of SiO_2 and $AlPO_4$, despite the fact that they share the same enantiomorphic space group. Our first-

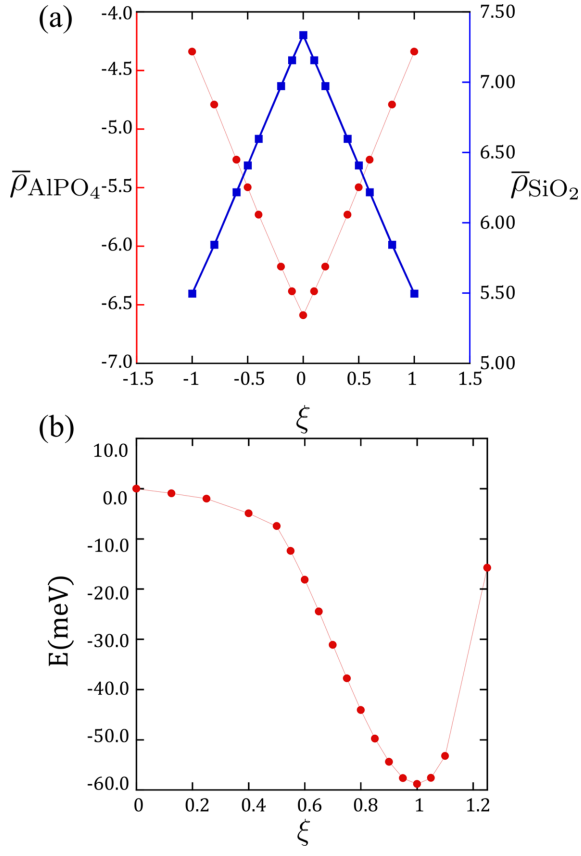

Figure 3
(*a*) Evolution of the rotatory power (in units of $^\circ\,mm^{-1}\,eV^{-2}$) as a function of the condensation of the Γ_3 mode distortion connecting the $P6_422$ and $P3_121$ phases of $AlPO_4$ and SiO_2. Red (left) and blue (right) axes correspond, respectively, to the rotatory power associated with the $AlPO_4$ and SiO_2 crystal structures. (*b*) Energy profile associated with the condensation of the unstable Γ_3 phonon mode eigendisplacement as calculated in SiO_2. The crystal cell parameters are linearly interpolated between the two minima to model intermediate configurations.

Table 5
Evolution of the optical rotatory power $\overline{\rho}$ in $^\circ\,mm^{-1}\,eV^{-2}$ computed from first principles as a function of the normalized amplitude of the Γ_3 distortion ξ from the $P6_422$ to the $P3_121$ phases of SiO_2 and $AlPO_4$.

The values at 0 and 1 correspond to the optimal $P6_422$ and $P3_121$ phases.

ξ	$\overline{\rho}_{SiO_2}$	$\overline{\rho}_{AlPO_4}$
−1.0	5.4973	−4.3400
−0.8	5.8443	−4.7913
−0.6	6.2176	−5.2621
−0.5	6.4082	−5.4975
−0.4	6.5985	−5.7297
−0.2	6.9731	−6.1746
−0.1	7.1562	−6.3856
0.0	7.3364	−6.5884
0.1	7.1562	−6.3856
0.2	6.9731	−6.1746
0.4	6.5985	−5.7297
0.5	6.4082	−5.4975
0.6	6.2176	−5.2621
0.8	5.8443	−4.7913
1.0	5.4973	−4.3400

principles calculations predict a positive rotatory power for the $P6_422$ and $P3_121$ phases of SiO_2 for light travelling along its optical axis, in agreement with Zabalo & Stengel (2023) (despite the handedness of the screw axis given in this space-group symbol), and a negative rotatory power for light travelling along its optical axis for the $P6_422$ and $P3_121$ phases of $AlPO_4$. The numerical values that we obtained for SiO_2 are in good agreement with the values encountered in the literature (Jönsson *et al.*, 1996), and the change in rotatory sign between SiO_2 and $AlPO_4$ is also consistent with a previous report by Glazer & Stadnicka (1986). This finding underscores a crucial concept: the sign of a crystal's NOA links to its structural chirality, although it might not align with the helical handedness indicated by the space-group symbol (Glazer & Stadnicka, 1986; Glazer & Stadnicka, 1989). This finding cautions against the common assumption that the sign of rotatory power unambiguously reflects the absolute sense of the principal screw axis (Tanaka *et al.*, 2010) even in materials with similar space groups.

We can trace and explain the difference in rotatory power by examining the crystal structures of both materials. As mentioned in the previous section and now shown in Fig. 4, the atomic positions of $AlPO_4$ in its $P6_422$ setting are very similar to those of the SiO_2 crystal in its $P6_222$ setting. In fact, when we perform a computational experiment by substituting the Si atoms onto the Al and P sites of the $AlPO_4$ structure and calculating the optical activity, we obtain a rotatory power with the opposite sign to that of SiO_2 in its $P6_422$ phase and that closely resembles that found for $AlPO_4$ in its $P6_222$ phase. Furthermore, upon relaxing the atomic positions in this modified structure, the system naturally evolves into the $P6_222$ phase of SiO_2, although initially a $P6_422$ symmetry is detected by *Abinit*. As discussed by Glazer & Stadnicka (1986) and Schwarzenbach (1966), similarly to quartz, three helical chains of oxygen atoms are identified, two left-handed and one right-handed. These chains, composed of the most polarizable atoms in the crystal (oxygen sites in this case), dominate the optical activity of these phases, thereby accounting for their

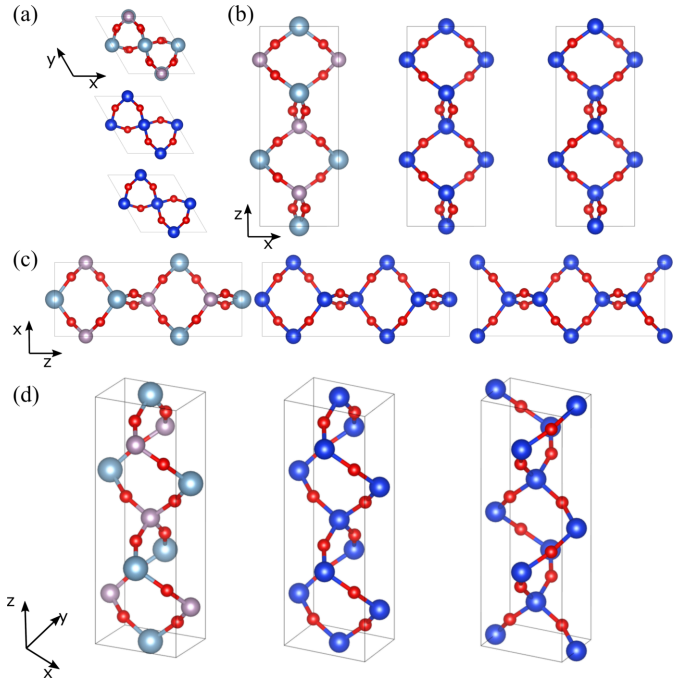

Figure 4
Comparison of the crystal structures of $P6_422$ $AlPO_4$, $P6_222$ SiO_2 and $P6_422$ SiO_2, ordered from top to bottom or left to right, respectively, in each case. The SiO_2 crystal structure has been duplicated along the c axis for comparison purposes. (*a*)–(*d*) Different views of the crystal structures as indicated by the corresponding Cartesian axis. Dark-blue, light-blue, pink and red balls correspond to Si, Al, P and O atoms, respectively.

observed rotatory power (Glazer & Stadnicka, 1986; Glazer & Stadnicka, 1989). Moreover, the observation that substituting Si atoms on the Al and P sites does not significantly alter the rotatory power suggests that these atomic species contribute little to the optical activity, confirming that it mainly arises from the more polarizable oxygen atoms.

The second interesting observation is that the condensation of the Γ_3 distortion decreases the value of the rotatory power in these types of transitions where the screw-axis type is reversed. Indeed, as shown in Fig. 3 we observe a linear decrease in the rotatory power as we condense the distortion. This can be explained by looking at the distortions shown in Figs. 1 and 2 that tend to disrupt the helical arrangement of the O atoms. One might expect that further increasing the amplitude of the distortion could eventually reverse the sign of the optical activity; however, our calculations show that, for instance, an amplitude 50% larger than the optimal value recovers rotatory power values comparable to those of the undistorted high-symmetry phase. Moreover, this increase in distortion amplitude is accompanied by a significant increase in the Landau energy, as shown in Fig. 3(*b*), indicating that such configurations are physically inaccessible.

4. Conclusion

In this work, we performed an *ab initio* analysis of the structural transitions and associated changes in the natural optical activity between the high-symmetry $P6_422$ ($P6_222$) and low-

symmetry $P3_121$ ($P3_221$) phases of SiO_2 and $AlPO_4$. Our first-principles calculations show that both materials undergo a displacive phase transition driven by the softening of a phonon mode at the zone centre with Γ_3 symmetry. This mode induces a distortion that reverses the sign of the principal screw axis of the crystal structure's high-symmetry space group.

Despite this reversal, the sense of the natural optical activity of the materials is preserved throughout the transition. $AlPO_4$ and SiO_2 therefore provide a useful illustration of the principle that it is the handedness of the most polarizable atoms in a structure that determines the sign of its natural optical activity (Glazer & Stadnicka, 1986; Glazer & Stadnicka, 1989). Upon cooling through its β–α phase transition, the screw sense of the imperfectly symmetric helix of oxygen sites is not changed (although this is not obvious from the space-group symmetries of the α and β phases, where the helix handedness given by the space-group symbol is reversed), preserving therefore the optical activity of the system.

Interestingly, the closely related structures of $AlPO_4$ and SiO_2 also highlight the role of the most polarizable oxide ions. The $AlPO_4$ and SiO_2 structures differ due to the ordering of Al and P sites in $AlPO_4$, which doubles the c axis of the unit cell. As a result, the space groups of the higher-symmetry phases are reversed (high-temperature $AlPO_4$ of $P6_422$ symmetry has atom sites, including those of the polarizable oxygens, close to those of SiO_2 of $P6_222$ symmetry). This means that the optical activity sign of $P6_422$ $AlPO_4$ is the same as that of $P6_222$ SiO_2.

Furthermore, our analysis of the Γ_3 transition pathway indicates a linear decrease in the magnitude of the rotatory power as the Γ_3 mode progresses from the high-symmetry to the low-symmetry phase for both SiO_2 and $AlPO_4$ crystals. This trend suggests that the symmetry lowering introduced by the distortion reduces the handedness of the structure (as shown in Fig. 3).

Our results highlight the intricate relationship between structural chirality and optical activity in chiral crystals and caution against simplistic interpretations based solely on space-group symmetry.

Funding information

Fernando Gómez-Ortiz acknowledges financial support from MSCA-PF 101148906 funded by the European Union and the Fonds de la Recherche Scientifique (FNRS) through grant No. FNRS-CR 1.B.227.25F. Fernando Gómez-Ortiz and Eric Bousquet acknowledge the Fonds de la Recherche Scientifique (FNRS) for financial support, the PDR project CHRYSALID No. 40003544 and the Consortium des Équipements de Calcul Intensif (CÉCI), funded by the FRS-FNRS under grant No. 2.5020.11, as well as computational resources made available on Lucia, the Tier-1 supercomputer of the Walloon Region, infrastructure funded by the Walloon Region under grant agreement No. 1910247. Fernando Gómez-Ortiz and Eric Bousquet also acknowledge support from the European Union's Horizon 2020 research and innovation programme under grant agreement No. 964931 (TSAR). We also recognize the support of the West Virginia Higher Education Policy Commission under the call Research Challenge Grand Program 2022 (award RCG 23-007) and NASA EPSCoR award 80NSSC22M0173.

References

Ades, S. & Champness, C. H. (1975). *J. Opt. Soc. Am.* **65**, 217.
Agranovich, V. M. & Ginzburg, V. (1984). *Crystal optics with spatial dispersion, and excitons.* New York: Springer-Verlag.
Antao, S. M. (2016). *Acta Cryst.* B**72**, 249–262.
Arago, F. (1811). *Mémoire sur la polarisation colorée.* Oeuvres complètes de François Arago.
Axe, J. D. & Shirane, G. (1970). *Phys. Rev. B* **1**, 342–348.
Barron, L. D. (2009). *Molecular light scattering and optical activity.* Cambridge University Press.
Biot, J. B. (1812). *Mem. Cl. Sci. Math. Phys. Inst.* **13**, 1.
Bousquet, E., Fava, M., Romestan, Z., Gómez-Ortiz, F., McCabe, E. E. & Romero, A. H. (2025). *J. Phys. Condens. Matter* **37**, 163004.
Campbell, B., Howard, C. J., Averett, T. B., Whittle, T. A., Schmid, S., Machlus, S., Yost, C. & Stokes, H. T. (2018). *Acta Cryst.* A**74**, 408–424.
Campbell, B. J., Stokes, H. T., Tanner, D. E. & Hatch, D. M. (2006). *J. Appl. Cryst.* **39**, 607–614.
Choudhury, N. & Chaplot, S. L. (2006). *Phys. Rev. B* **73**, 094304.
Condon, E. U. (1937). *Rev. Mod. Phys.* **9**, 432–457.
Dolino, G., Bachheimer, J.-P., Gervais, F. & Wright, A. F. (1983). *Bull. Minéral.* **106**, 267.
Donnay, J. D. H. & Le Page, Y. (1978). *Acta Cryst.* A**34**, 584–594.
Erb, K. C. & Hlinka, J. (2018). *Phase Transit.* **91**, 953–958.
Fava, M., McCabe, E., Romero, A. H. & Bousquet, E. (2024). *arXiv*, 2405.12696 [cond-Mater. mtrl-Sci].
Fecher, G. H., Kübler, J. & Felser, C. (2022). *Materials* **15**, 5812.
Glazer, A. M. (2018). *J. Appl. Cryst.* **51**, 915–918.
Glazer, A. M. & Stadnicka, K. (1986). *J. Appl. Cryst.* **19**, 108–122.
Glazer, A. M. & Stadnicka, K. (1989). *Acta Cryst.* A**45**, 234–238.
Gómez-Ortiz, F., Fava, M., McCabe, E. E., Romero, A. H. & Bousquet, E. (2024). *Phys. Rev. B* **110**, 174112.
Gómez-Ortiz, F., Romero, A. H. & Bousquet, E. (2025). *arXiv*, 2503.13076 [cond-Mater. mtrl-Sci].
Gonze, X., Amadon, B., Antonius, G., Arnardi, F., Baguet, L., Beuken, J.-M., Bieder, J., Bottin, F., Bouchet, J., Bousquet, E., Brouwer, N., Bruneval, F., Brunin, G., Cavignac, T., Charraud, J.-B., Chen, W., Côté, M., Cottenier, S., Denier, J., Geneste, G., Ghosez, P., Giantomassi, M., Gillet, Y., Gingras, O., Hamann, D. R., Hautier, G., He, X., Helbig, N., Holzwarth, N., Jia, Y., Jollet, F., Lafargue-Dit-Hauret, W., Lejaeghere, K., Marques, M. A., Martin, A., Martins, C., Miranda, H. P., Naccarato, F., Persson, K., Petretto, G., Planes, V., Pouillon, Y., Prokhorenko, S., Ricci, F., Rignanese, G.-M., Romero, A. H., Schmitt, M. M., Torrent, M., van Setten, M. J., Van Troeye, B., Verstraete, M. J., Zérah, G. & Zwanziger, J. W. (2020). *Comput. Phys. Commun.* **248**, 107042.
Gonze, X. & Lee, C. (1997). *Phys. Rev. B* **55**, 10355–10368.
Grimm, H. & Dorner, B. (1975). *J. Phys. Chem. Solids* **36**, 407–413.
Halasyamani, P. S. & Poeppelmeier, K. R. (1998). *Chem. Mater.* **10**, 2753–2769.
Hamann, D. (2013). *Phys. Rev. B* **88**, 085117.
Hlinka, J. (2014). *Phys. Rev. Lett.* **113**, 165502.
Iwasaki, H., Sugii, K., Niizeki, N. & Toyoda, H. (1972). *Ferroelectrics* **3**, 157–161.
Jerphagnon, J. & Chemla, D. S. (1976). *J. Chem. Phys.* **65**, 1522–1529.
Jönsson, L., Levine, Z. H. & Wilkins, J. W. (1996). *Phys. Rev. Lett.* **76**, 1372–1375.
Kizel', V. A. (1980). *Sov. Phys. Usp.* **23**, 277–295.
Landau, L. D. & Lifshitz, E. M. (1984). *Electrodynamics of continuous media*, Course of theoretical physics, Vol. 8, 2nd ed. Pergamon.

Malashevich, A. & Souza, I. (2010). *Phys. Rev. B* **82**, 245118.
Muraoka, Y. & Kihara, K. (1997). *Phys. Chem. Miner.* **24**, 243–253.
Natori, K. (1975). *J. Phys. Soc. Jpn* **39**, 1013–1021.
Ng, H. N. & Calvo, C. (1976). *Can. J. Phys.* **54**, 638–647.
Nomura, K. C. (1960). *Phys. Rev. Lett.* **5**, 500–501.
Pozo Ocaña, Ó. & Souza, I. (2023). *SciPost Phys.* **14**, 118.
Raman, C. V. & Nedungadi, T. M. K. (1940). *Nature* **145**, 147.
Schwarzenbach, D. (1966). *Z. Kristallogr.* **123**, 161–185.
Shapiro, S. M., O'Shea, D. C. & Cummins, H. Z. (1967). *Phys. Rev. Lett.* **19**, 361–364.
Stokes, H. T., Hatch, D. M. & Campbell, B. J. (2025). *ISODISTORT*, in *ISOTROPY software suite*, https://iso.byu.edu.
Tanaka, Y., Kojima, T., Takata, Y., Chainani, A., Lovesey, S. W., Knight, K. S., Takeuchi, T., Oura, M., Senba, Y., Ohashi, H. & Shin, S. (2010). *Phys. Rev. B* **81**, 144104.
Tezuka, Y., Shin, S. & Ishigame, M. (1991). *Phys. Rev. Lett.* **66**, 2356–2359.
Thong, N. & Schwarzenbach, D. (1979). *Acta Cryst.* A**35**, 658–664.
Urru, A., Souza, I., Ocaña, P., Tsirkin, S. S. & Vanderbilt, D. (2025). *Phys. Rev. B* **112**, 045201.
van Setten, M. J., Giantomassi, M., Bousquet, E., Verstraete, M. J., Hamann, D. R., Gonze, X. & Rignanese, G.-M. (2018). *Comput. Phys. Commun.* **226**, 39–54.
Wang, X. & Yan, Y. (2023). *Phys. Rev. B* **107**, 045201.
Wooster, W. A. (1953). *Rep. Prog. Phys.* **16**, 62–82.
Zabalo, A. & Stengel, M. (2023). *Phys. Rev. Lett.* **131**, 086902.
Zhong, H., Levine, Z. H., Allan, D. C. & Wilkins, J. W. (1993). *Phys. Rev. B* **48**, 1384–1403.